Physics of the Earth and Planetary Interiors 283 (2018) 38–42

Contents lists available at ScienceDirect

Physics of the Earth and Planetary Interiors

journal homepage: www.elsevier.com/locate/pepi

Ultrasonic acoustic wave velocities of neighborite ($NaMgF_3$) across orthorhombic to cubic phase boundary at high P-T

Li Li*, Donald J. Weidner, Matthew L. Whitaker, Richard Triplett

Mineral Physics Institute, Stony Brook University, Stony Brook, NY, USA

A B S T R A C T

Neighborite perovskite ($NaMgF_3$) is a close analogue to Mg or Ca silicate perovskite. It experiences a second-order phase transition at high T that may have a significant effect on the acoustic velocities. Here we report the measurement of elastic wave velocities of neighborite perovskite using the multi-anvil high-pressure apparatus located in beamline 6-BM-B at the Advanced Photon Source. We use the newly installed ultrasonic interferometry equipment using pulse-echo-overlap method coupled with the D-DIA device. X- radiographic imaging is used to measure sample length at high P-T. X-ray diffraction spectrum is used to determine the pressure and sample conditions. Precise measurements of P and S wave velocities are at 60 and 35 MHz respectively and are nearly simultaneous. We use a double reflector method to enable measurement of elastic wave velocities of cold-pressed polycrystalline sample that is sintered in situ at high P-T. Experiments were carried out up to 3 GPa and 1000 °C. Our results indicated that MHz ultrasonic acoustic velocities experience a significant minimum at the phase transition, with the bulk modulus being more affected than the shear modulus. The shear modulus of the cubic phase appears unchanged from those of the orthorhombic phase, while the bulk modulus increases in transforming into the cubic phase.

1. Introduction

Silicate perovskite, the host of almost all of the Si in the lower mantle, makes up nearly half of the Earth's volume. The characterization of the physical properties of this phase is thus crucial in modeling the composition and dynamics of Earth's deep interior. Many materials with the perovskite structure demonstrate continuous structural distortion and displacive phase transitions with changing pressure and temperature (Glazer, 1972, 1975; Aleksandrov, 1976, 1978, Liu et al., 2005). These structural phase transitions in perovskites can introduce changes in acoustic velocity, thermal expansion, and electrical conductivity, as well as changes in rheological properties (Salje, 1989) that occur both in the neighborhood of the transition as well as between two phases. The effect of pressure and temperature on structural distortions and phase transitions is thus important in determining the physical properties and stability of perovskite materials.

$NaMgF_3$ (neighborite) is a close analogue to $MgSiO_3$ perovskite. They are isostructural and isoelectronic due to the comparable ionic radii and electronic charge ratio for ions. The weak bonding strength of $NaMgF_3$ perovskite results in the major phase transitions occurring at lower pressure and temperatures; thus, experimentally more accessible. Neighborite experiences an orthorhombic to cubic phase transformation along a univariant curve in P-T space. The acoustic velocity variation during this second-order phase transition is a strongly coupled phonon softening process but still not experimentally quantified for neighborite. Here we report experimental determinations of the acoustic velocities across this transformation.

Neighborite is an ABX_3 orthorhombic perovskite, with Mg in the octahedral site and Na in the larger, 12 coordinated site. The orthorhombic version is distorted from the cubic aristotype by rotation of the BX6 octahedra (Glazer, 1972, 1975) about each of the three cubic axes. The octahedral rotations can be in-phase as noted by $\varnothing_z^+$ for rotation about the z axis or anti-phase as indicated by $\varnothing_x^-$ as about the x axis. The orthorhombic *Pbnm* (, Z = 4) is defined by equal anti- phase rotations about the x and y axes with an in-phase rotation about the z axis. The unit cell of the orthorhombic phase is rotated to the (1, 1, 0) cubic direction and the size of the unit cell quadruples over that of the cubic structure. At elevated temperature the orthorhombic perovskite transforms to the cubic, $Pm\bar{3}m$, (000) with both systems of octahedral rotations diminishing to zero at the same temperature. For most perovskites, these two distortions will vanish with increasing temperature, but at different temperatures forming an intermediate tetragonal phase. Critical phenomena have been reported during these second order phase transitions in properties such as thermal expansion and heat capacity. Not only is there often softening of elastic moduli at the point of the transition, but also an offset in properties from one phase relative to another.

In this study, we report the MHz sound velocities of $NaMgF_3$ perovskite through the orthorhombic-cubic phase boundary at high pressure and temperature. X-ray diffraction spectra were collected during the experiment to monitor the stress state and crystal structure.

* Corresponding author.
E-mail addresses: li.li.2@stonybrook.edu, lili.stonybrook@gmail.com (L. Li).

https://doi.org/10.1016/j.pepi.2018.08.002
Received 18 April 2018; Received in revised form 17 July 2018; Accepted 5 August 2018
Available online 06 August 2018
0031-9201/ Published by Elsevier B.V.

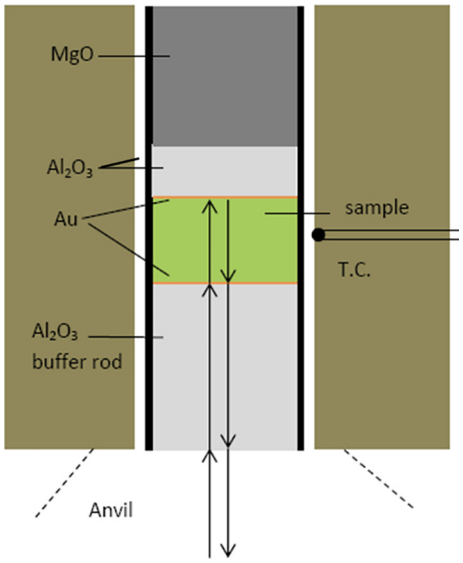

Fig. 1. High pressure ultrasonic cell assembly. The sample occupies a cylindrical hole in the amorphous-boron epoxy 6 mm cube. The cylindrical hole is lined with a corundum sleeve with a graphite sleeve inside that is the heater. From the bottom is a corundum buffer rod of 2.35 mm length and 2.5 mm diameter, polished on both ends with a 1 μm gold foil on the polished surface. The sample of length 1.2 mm is above the buffer rod and a corundum reflector of length 0.72 mm is above the sample. The sample side of the reflector is polished and the interface is lined with a 1 μm thick gold foil. An MgO plug fills in the rest of the cylinder.

2. Experimental method

High pressure and high temperature experiments were carried out using the system for in situ ultrasonic measurement using phase comparison, installed at beamline 6-BM-B in the synchrotron X-ray radiation facility of Advanced Photon Source, Argonne National Lab (see (Whitaker et al., 2017)). The multi-anvil high pressure device D-DIA provides a controlled pressure and temperature environment. Tungsten carbide and sintered diamond anvils with 4 mm truncation were used. The 10-element Ge solid-state detector array was at a fixed Bragg angle of 2θ close to 6.5. A CCD imaging camera focused on a YAG scintillator was used to monitor the sample length from X-ray radiographs. 1 μm thick gold foils were used to mark the sample boundary. The $NaMgF_3$ perovskite sample is a polycrystalline sample with grain size about 5 μm. The cold pressed sample cylinder is about 2.5 mm in diameter and 1.2 mm long. The sample is placed in a high-pressure cell with a graphite furnace and boron epoxy pressure medium (see Fig. 1). A polished dense alumina cylinder 2.5 mm diameter and 2.35 mm length is used as the buffer rod sandwiched between the anvil and the sample. The top of the sample is in contact with the polished surface of a second alumina cylinder, the reflector, 0.72 mm long. Above the second alumina rod is MgO powder. The ultrasonic signals were generated by the $LiNbO_3$ transducer. Acoustic velocities are determined by comparing arrival times of echoes from the buffer rod – sample interface with those from the sample – reflector interface. We use the DIASCoPE ultrasonic system (Whitaker et al., 2017) to measure P and S velocities by measuring round-trip travel times in the sample using the phase comparison technique (Li, 2009). P wave signals are from a 5 cycle sine wave burst of 60 MHz, S waves are at 35 MHz. P and S wave data are taken within about 1 s of each other, using the same 10° Y-cut piezoelectric transducer.

Temperature is obtained from the heater power and previous power vs temperature calibrations. We estimate the temperature accuracy to about 50 °C and expect as much as a 50 °C temperature variation within the cell (Raterron et al., 2013). Pressure is defined using the unit cell volume of the corundum buffer rod from X-ray diffraction measurements along with appropriate equation of state variables. With this calibration, our temperature corresponding to the phase transition as defined by the disappearance of the superlattice reflections agreed to within 15 °C of that reported by (Martin, 2007) using the same criterion.

Pressure is initially increased to about 3 GPa and the oil pressure is held constant during the run. Temperature is increased to 225 °C where it is held for about an hour and then increased in steps by 10–20 degrees per step, taking ultrasonic data, image data, and diffraction data on both the sample and the corundum buffer rod up to about 900 °C. Each step took a total of about 6 min. By 600 °C the stresses in the sample significantly relaxed as evidenced by the peak broadening of the diffraction data. This is generally achieved after the porosity has been eliminated due to collapse and annealing (Weidner et al., 1994). Finally, at the maximum temperature, the sample is quenched.

3. Results

3.1. X-ray diffraction

The orthorhombic structure is slightly distorted from the cubic structure. Thus, diffraction peaks that arise from many high symmetry reflections like (200) which are at the same two theta as (020) and (002) in the cubic phase, will reflect different lattice spacings in the orthorhombic structure. Thus, the cubic peak, (200) will be split into three peaks in the orthorhombic structure, but the peaks may be close enough in d-spacing that they appear as a broadened peak. Furthermore, the cubic setting is 45° rotated from the orthorhombic setting, making the *hkl* designation of the peaks different in the two symmetries. While the orthorhombic structure becomes closer to the cubic structure as the rotation angles approach zero, the multiple peaks will merge into one peak with an apparent narrowing of the diffraction peak.

In addition, in the cubic structure there will be systematic absences of peaks for some *hkl* values owing to the high symmetry of the crystal. As the symmetry is reduced by the distortion, these systematic absences will become real peaks designated as superlattice reflections. The superlattice diffraction peaks of the distorted perovskite structure that result from octahedral tilting disappear as the orthorhombic phase transforms to cubic. For the supercell *Pbnm* (, Z = 4), the three diffraction peaks $\{121, 103, 211\}_{Pbnm}$ indicates the anti-phase tilting, while $\{120, 210\}_{Pbnm}$ and $\{122, 212\}_{Pbnm}$ indicates the in-phase tilting. Vanishing of either set of peaks indicates a transformation from the orthorhombic phase to a tetragonal phase; vanishing of both sets of peaks indicates transformation to cubic. Fig. 2 illustrates the diffraction pattern taken at 830 °C and 847 °C. The data presented here are the summation of the diffraction spectra over 8 detectors that are aligned to the same sample volume and simultaneously recording the data. The dark lines reflect the position and amplitude of the diffraction peaks for the orthorhombic phase from the jcpds data set. The location of the three sets of superlattice peaks are indicated along with two peaks that persist in the cubic structure. The reflections are identified by their *Pbnm* reference frame. The superlattice peaks all disappear between the two temperatures. We consider that the orthorhombic to cubic phase transition occurred at a temperature between these two temperatures. Fig. 3 illustrates the intensity of these three peaks as a function of temperature demonstrating the rather abrupt disappearance of these peaks.

Fig. 4 illustrates the apparent peak width of the $\{200, 020, 112\}_{Pbnm}$ triplet. Also illustrated here is the temperature where the superlattice reflections disappear. We find that at this same temperature, the triplet obtained a stable peak width. We conclude that the disappearance of the superlattice peaks is the most definitive criteria to define the change in crystal structure, and it is compatible with the merging of split peaks into a single peak. We further confirm that within the uncertainty of these experiments, the phase transition is

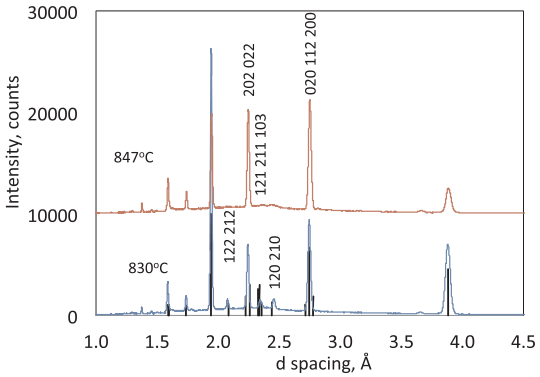

Fig. 2. X-ray diffraction patterns of the neighborite sample both before (830 °C) and after (847 °C) the orthorhombic to cubic phase transformation. This pattern represents the sum over 8 detectors that collect data simultaneously from the conical slit system. The (*hkl*) identifications in the orthorhombic coordinate system are indicated above some of the diffraction lines. In the orthorhombic phase these are usually more than one diffraction line, but with very similar lattice spacings. In the cubic phase, these converge to single peaks. The three diffraction peaks, $\{121, 103, 211\}_{Pbnm}$, $\{120, 210\}_{Pbnm}$, and $\{122, 212\}_{Pbnm}$ disappear in the cubic phase.

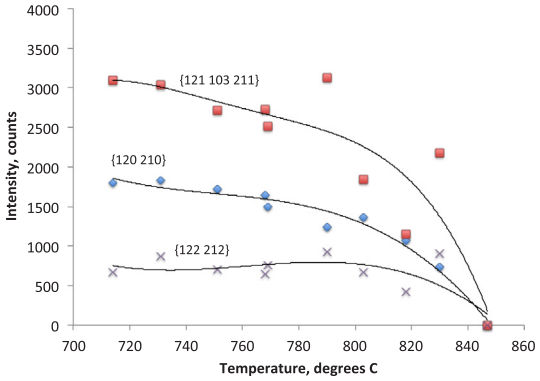

Fig. 3. Amplitude of the superlattice reflections as a function of temperature. The three superlattice reflections vanish at the same temperature, 847 °C. This indicates that both order parameters vanish at the same time with a direct transformation from orthorhombic to cubic with no intermediate tetragonal phase.

orthorhombic to cubic with no evidence of an intermediate tetragonal phase.

3.2. Ultrasonic properties

Measured P and S velocities are illustrated in Fig. 5 as a function of temperature. The phase transition identified by the disappearance of the superlattice reflections at 847 °C is preceded by a local velocity minimum at 790 °C for both the P and S waves. While the data in Fig. 5 is plotted as a function of temperature, we note that the pressure was varying with temperature even though the loading force was held constant. Fig. 6 represents the bulk and shear modulus that have been extracted from the velocity data and corrected to zero pressure using a pressure derivative of the bulk modulus, K', of 4.5, and for the shear modulus, μ', of 1.5. Also illustrated in Fig. 6 are the room temperature, zero pressure bulk and shear moduli from Brillouin scattering (Zhao and Weidner, 1993) and the pressure-corrected elastic moduli from (Martin, 2007). All of the data of (Martin, 2007) are in the low temperature orthorhombic phase even though they were collected at higher temperature than our orthorhombic to cubic phase transition as they were collected at higher pressure than our data and remained on the low temperature side of the phase boundary. Thus, they define a useful

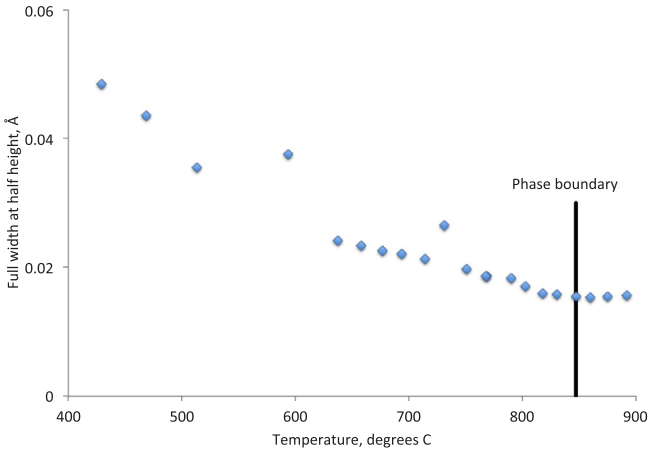

Fig. 4. The apparent peak width of the $\{200, 020, 112\}_{Pbnm}$ triplet as a function of temperature. This triplet is one of the larger peaks in the orthorhombic phase and converges to a singlet in the cubic phase. The three peaks merge into an apparent single peak when close to the phase boundary, but is widened by virtue of being 3 peaks. After the phase boundary, the peak width stabilizes indicating that the width is now dominated by the system resolution. The temperature of the phase boundary is indicated by the vertical black line.

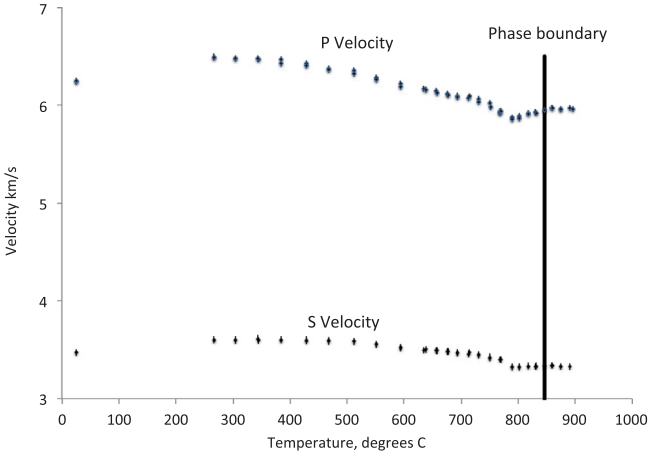

Fig. 5. Acoustic velocity as a function of temperature. These are the raw data without correction for the variation of pressure. The temperature of the phase boundary is indicated by the vertical black line.

baseline for the orthorhombic phase at conditions where we have the cubic phase. We note that our data agree well with the results of (Martin, 2007) for the orthorhombic phase in the neighborhood of the phase transition, but differ somewhat at lower temperatures. Our data, back extrapolated to room temperature, agree very well with the room temperature values of (Zhao and Weidner, 1993) especially considering that at temperatures below 600 °C our sample has not been totally compacted. As with the acoustic velocities, the elastic moduli exhibit a minimum at 790 °C, in advance of the disappearance of the superlattice reflections. As we go to the cubic phase, we find that the shear modulus is little changed from the orthorhombic phase as inferred from the data of (Martin, 2007), but the bulk modulus increases significantly indicating that the cubic phase has a similar shear modulus, but an enhanced bulk modulus compared to the orthorhombic phase.

Fig. 7 illustrates the amplitudes of the shear (S Wave) and longitudinal (P Wave) reflections as a function of temperature through the orthorhombic phase transition. The S wave signal exhibits a much stronger minimum than does the P wave and it is at the same temperature as the minimum shear velocity, while the P wave has a weaker, broader minimum at a slightly higher temperature. The amplitudes of both wave types recover by the temperature where the superlattice

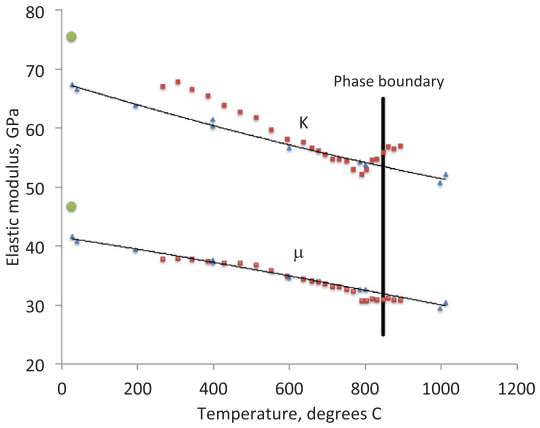

Fig. 6. Bulk and shear modulus as a function of temperature corrected to zero pressure with a K' = 4.5 and a μ = 1.5 illustrated by red squares. The room temperature, zero pressure bulk and shear moduli from Brillouin scattering of (Zhao and Weidner, 1993) are indicated by green circles at room temperature. The pressure-corrected elastic moduli of (Martin, 2007) are illustrated by blue crosses and fit to a linear solid line illustrated in black. All of the data of (Martin, 2007) are in the low temperature orthorhombic phase even though they were collected at higher temperature than our orthorhombic to cubic phase transition as they were collected at higher pressure than our data and remained on the low temperature side of the phase boundary. Our data, back extrapolated to room temperature, agree very well with the room temperature values of (Zhao and Weidner, 1993) especially considering that at temperature below 600 °C, our sample has not been totally compacted. As with the acoustic velocities, the elastic moduli exhibit a minimum at 790 °C, in advance of the disappearance of the superlattice reflections indicated by the black vertical line.

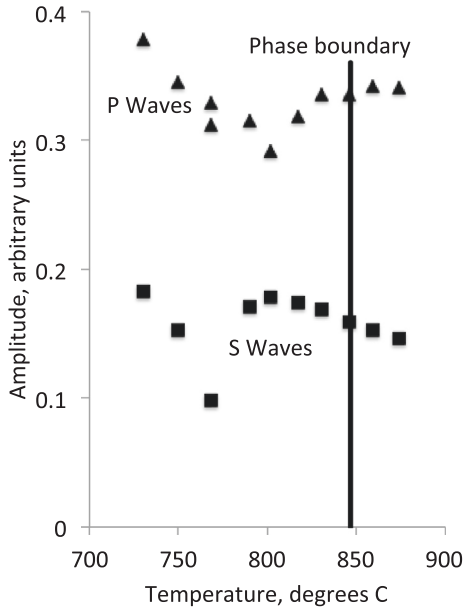

Fig. 7. The amplitudes of the shear (S Wave) and longitudinal (P Wave) reflections as a function of temperature through the orthorhombic to cubic phase transition. The S wave signal exhibits a much stronger minimum that does the P wave and it is at the same temperature as the minimum shear velocity, while the P wave has a weaker, broader minimum at a slightly higher temperature. The temperature of the phase boundary is indicated by the vertical black line.

reflections disappear and the sample is in the cubic phase. The amplitudes of these waves reflects a complex combination of phenomena that are not easily deconvolved. First, since velocity is varying with temperature in this region, then so is the acoustic impedance. As we are looking at reflected and transmitted waves, the changing impedance implies variations in wave amplitudes. Second, scattering from heterogeneities will cause loss of wave intensity. Near the transition, the size and distributions of twin domains may vary in the sample, causing changes in heterogeneous elastic properties. Finally, attenuation associated with the twinning process can absorb energy from the wave. In addition, the P waves are at 60 MHz, while the S waves are at 35 MHz allowing a different temperature effect on absorption or scattering for the two wave types. The major points concerning wave intensity are 1) the S waves experience a greater relative effect than the P waves, 2) the largest energy loss is nearly at the same temperature as the minimum velocity, 3) this temperature is significantly less than the orthorhombic to cubic transition as evidenced by the loss of the superlattice reflections.

4. Discussion

The change in space group from $Pm\bar{3}m$ (cubic) to *Pbnm* (orthorhombic) with lowering of temperature, in $NaMgF_3$, marks the ferroelastic phase transition in this 'improper' ferroelastic material caused by the rotation of rigid octahedra (Carpenter, 2006; Carpenter et al., 2006). Neighborite belongs to a group of perovskites in which this transformation is the result of slight rotations of the octahedra from their cubic position. With the rotation, the size of the large cation site is reduced and the structure itself assumes a macroscopic shear strain, the spontaneous strain. Twins are generated in which the rotation angle, and hence the spontaneous strain, differs in sign (Carpenter et al., 2001). As the rotation angle is small, the shear modulus associated with that shear is softened with associated attenuation. In addition, the stress can force a change from one twin state to another (Carpenter, 2015; Harrison and Redfern, 2002; Harrison et al., 2004; Li and Weidner, 2012) absorbing energy, thus lowering Q. This is consistent with our observations of softening of both the bulk and shear modulus in advance of the structural transition as indicated by the vanishing of the super lattice reflections as well as increased attenuation. The two mechanisms may affect bulk and shear differently with the resultant difference between the P wave Q and the S wave Q.

Neighborite exhibits some features that differ from the norm of this group of perovskites. First, there are two independent rotational angles that vanish along the P-T line that defines the phase transition, thereby eliminating an intermediate tetragonal phase (Zhao et al., 1994, 1993a,b). This suggests a strong coupling between the two order parameters and should heighten the effects of two phase transitions combined into one.

A second characteristic of the neighborite transition is the apparent shortening of the Mg-F bond length by about 2%, from X-ray diffraction, with increasing temperature over a small range as the orthorhombic phase transforms to cubic (Zhao et al., 1994). In apparent contradiction, total X-ray scattering via pair distribution function, yield an Mg-F distance that does not decrease with temperature in this region (Martin et al., 2007). The molecular dynamics result of (Street et al., 1997) help resolve this by demonstrating that the thermal vibrations are correlated, allowing the Mg-F bond to be longer than half of the F-F distance in the unit cell. (Li et al., 2006) studied the molecular dynamics of $CaSiO_3$ using density functional interaction models. By fitting rotational angles to each frame of the calculated structure, they found that the rotation angle for a stable structure began to jump from plus to minus as the thermal energy increased. The marking of a phase transition would then be the point where this jumping was enough to yield an average distortion angle of zero. They found that even at several thousand degrees, fitting a distortion angle to the atom positions significantly lowered the variance in an RMS fitting of the departure of atom positions from the cubic structure. The implication is that the cubic structure of neighborite may be a dynamic feature and that at any instant, the crystal structure is orthorhombic. The potential coupling of Mg-F bond lengths and a dynamic character to the phase transition couples the ferroelastic transition with volume driven properties. This may be the reason that the bulk modulus appears to be significantly

affected by the transition, having a significant softening as well as a major increase in association with the transition to cubic.

In this paper, we simultaneously measure X-ray diffraction and acoustic velocities of neighborite with increasing temperature across this phase boundary. The results are generally in accord with that expected for a ferroelastic perovskite such as neighborite. The diffraction data define the space group. The superlattice reflections reveal the lower symmetry and support the contention that there is no intermediate tetragonal phase. We further observe that softening in both the bulk modulus and the shear modulus occurs at temperatures somewhat lower than the formation of the cubic phase coupled with a modest attenuation of both the P and S waves. The shear modulus of the cubic phase appears indistinguishable from that of the orthorhombic phase outside of the softened region. The most remarkable feature is that the bulk modulus increases by about 7% in the cubic phase relative to that of the orthorhombic phase. This differs from a more normal transformation where the effect is greater on the shear modulus than on the bulk modulus (Carpenter et al., 2007). Perhaps the apparent shortening of the Mg-F bond contributes to this increase of bulk modulus in the cubic phase.

Acknowledgements

This research used resources of the Advanced Photon Source, a U.S. Department of Energy (DOE) Office of Science User Facility operated for the DOE Office of Science by Argonne National Laboratory under Contract No. DE-AC02-06CH11357 on beamline 6BMB with the support of Haiyan Chen. The research was supported by National Science Foundation of the United States grants EAR 1361463 and EAR 1547556 (LL and DJW). This research was partially supported by COMPRES, the Consortium for Materials Properties Research in Earth Sciences under NSF Cooperative Agreement EAR 1606856. The authors thank C. David Martin for neighborite starting material.

Appendix A. Supplementary data

Supplementary data associated with this article can be found, in the online version, at https://doi.org/10.1016/j.pepi.2018.08.002.

References

Aleksandrov, K.S., 1976. The sequences of structural phase transitions in perovskites. Ferroelectrics 16, 801–805.
Aleksandrov, K.S., 1978. Mechanisms of the ferroelectric and structural phase transitions: structural distortion in perovskites. Ferroelectrics 20, 61–67.
Carpenter, M.A., 2006. Elastic properties of minerals and the influence of phase transitions. Am. Mineral. 91 (2–3), 229–246. https://doi.org/10.2138/am.2006.1979.
Carpenter, M.A., 2015. Static and dynamic strain coupling behaviour of ferroic and multiferroic perovskites from resonant ultrasound spectroscopy. J. Phys.-Condens. Matter 27 (26). https://doi.org/10.1088/0953-8984/27/26/263201.
Carpenter, M.A., Becerro, A.I., Seifert, F., 2001. Strain analysis of phase transitions in (Ca, Sr)TiO3 perovskites. Am. Mineral. 86 (3), 348–363.
Carpenter, M.A., Sondergeld, P., Li, B.S., Liebermann, R.C., Walsh, J.W., Schreuer, J., Darling, T.W., 2006. Structural evolution, strain and elasticity of perovskites at high pressures and temperatures. J. Mineral. Petrol. Sci. 101 (3), 95–109. https://doi.org/10.2465/jmps.101.95.
Carpenter, M.A., Li, B.S., Liebermann, R.C., 2007. Elastic anomalies accompanying phase transitions in (Ca, Sr)TiO(3) perovskites: part III. Experimental investigation of polycrystalline samples. Am. Mineral. 92 (2–3), 344–355. https://doi.org/10.2138/am.2007.2297.
Glazer, A.M., 1972. The classification of tilted octahedra in perovskites. Acta Cryst. B28, 3384.
Glazer, A.M., 1975. Simple ways of determining perovskite strucutres. Acta Cryst. A31, 756.
Harrison, R.J., Redfern, S.A., 2002. The influence of transformation twins on the seismic-frequency elastic and anelastic properties of perovskite: dynamical mechanical analysis of single crystal LaAlO3. Phys. Earth Planet. Inter. 134 (3–4), 253–272. https://doi.org/10.1016/s0031-9201(02)00190-5.
Harrison, R.J., Redfern, S.A.T., Salje, E.K.H., 2004. Dynamical excitation and anelastic relaxation of ferroelastic domain walls in LaAlO3. Phys. Rev. B 69 (14).
Li, B., 2009. Precise sound velocity measurements on solids and liquids at high pressure and high temperature with direct length measurement. J. Acoust. Soc. Am. 125 (4), 2653.
Li, L., Weidner, D.J., Brodholt, J., Alfè, D., Price, G.D., Caracas, R., Wentzcovitch, R., 2006. Phase stability of $CaSiO_3$ perovskite at high pressure and temperature: insights from ab initio molecular dynamics. Phys. Earth Planet. Sci. 155 (3–4), 260–268.
Li, L., Weidner, D.J., 2012. Anelasticity and transient creep in NaMgF3 perovskite at high pressure. Phys. Earth Planet. Inter. 194, 98–106. https://doi.org/10.1016/j.pepi.2012.01.009.
Liu, H.Z., Chen, J., Hu, J., Martin, C.D., Weidner, D.J., Hausermann, D., Mao, H.K., 2005. Octahedral tilting evolution and phase transition in orthorhombic NaMgF3 perovskite under pressure. Geophys. Res. Lett. 32 (4). https://doi.org/10.1029/2004gl022068.
Martin, C.D., 2007. Structure and Elasticity of NaMgF3 and CaIrO3 at High Pressures and Temperatures—The Perovskite and Post-Perovskite Structure Model of MgSiO3 Investigated with Rietveld Structure Refinement and Ultrasonic. Stony Brook.
Martin, C.D., Chupas, P.J., Chapman, K.W., Parise, J.B., 2007. Local versus average structure: a study of neighborite (NaMgF3) utilizing the pair distribution function method for structure determination. J. Appl. Crystallogr. 40, 441–448. https://doi.org/10.1107/ s0021889807014148.
Raterron, P., Merkel, S., Holyoke, C.W., 2013. Axial temperature gradient and stress measurements in the deformation-DIA cell using alumina pistons. Rev. Sci. Instrum. 84 (4). https://doi.org/10.1063/1.4801956.
Salje, E., 1989. Characteristics of perovskite-related materials. Philos. Trans. R. Soc. London, Sect A 328, 409–416.
Street, J.N., Wood, I.G., Knight, K.S., Price, G.D., 1997. The influence of thermal vibrations on the average structure of cubic NaMgF(3) perovskite: a combined molecular dynamics and neutron diffraction study. J. Phys.-Condens. Matter 9 (50), L647–L655. https://doi.org/10.1088/0953-8984/9/50/001.
Weidner, D.J., Wang Y., and Vaughan M. T., 1994. Deviatoric stress measurements at high pressure and temperature, In: Schmidt S.C., Shaner J.W., Samara G. A. and Ross M. (Eds.), High-Pressure Science and Technology (Proceedings of the 1993 AIRAPT Conference), 1025–1028.
Whitaker, M.L., Baldwin, K.J., Huebsch, W.R., 2017. DIASCoPE: directly integrated acoustic system combined with pressure experiments-a new method for fast acoustic velocity measurements at high pressure. Rev. Sci. Instrum. 88 (3), 8. https://doi.org/10.1063/1.4977596.
Zhao, Y.S., Parise, J.B., Wang, Y.B., Kusaba, K., Vaughan, M.T., Weidner, D.J., Kikegawa, T., Chen, J., Shimomura, O., 1994. High-pressure crystal-chemistry of neighborite, NaMgF3 - an angle-dispersive diffreaction study using monochromatic synchrotron X-radiation. Am. Mineral. 79 (7–8), 615–621.
Zhao, Y., Weidner, D.J., 1993. The single crystal elastic moduli of neighborite. Phys. Chem. Miner. 20, 419–424.
Zhao, Y.S., Weidner, D.J., Parise, J.B., Cox, D.E., 1993a. Critical phenomena and phase-transition of perovskite: data for NaMgF3 perovskite. 2. Phys. Earth Planet. Inter. 76 (1–2), 17–34. https://doi.org/10.1016/0031-9201(93)90052-b.
Zhao, Y.S., Weidner, D.J., Parise, J.B., Cox, D.E., 1993b. Thermal-expansion and structural distortion of perovskite - data for NaMgF3 perovskite. 1. Phys. Earth Planet. Inter. 76 (1–2), 1–16. https://doi.org/10.1016/0031-9201(93)90051-a.